Accepted manuscript.
Final publication is available from Mary Ann Liebert, Inc., publishers http://dx.doi.org/10.1089/brain.2019.0668

A novel method for extracting hierarchical functional subnetworks based on a multi-subject spectral clustering approach

Xiaoyun Liang[a,b], Chun-Hung Yeh[a], Alan Connelly[a,c], Fernando Calamante[a,c,d]

[a] *The Florey Institute of Neuroscience and Mental Health, Heidelberg, Victoria, Australia.*

[b]*Mary Mackillop Institute for Health Research, Australian Catholic University, Melbourne, Victoria, Australia*

[c] *The Florey Department of Neuroscience and Mental Health Medicine, University of Melbourne, Melbourne, Victoria, Australia*

[d] *The University of Sydney, Sydney Imaging, and School of Aeronautical, Mechanical and Mechatronic Engineering, Sydney, New South Wales, Australia*

Running title: Group-level spectral clustering of hierarchical subnetworks

Word count: 4998

Correspondence to: Xiaoyun Liang, PhD

Florey Institute of Neuroscience and Mental Health

Melbourne Brain Centre

245 Burgundy St.

Heidelberg

Victoria, 3084, Australia

Telephone: (+61 3) 9035 7159

Fax: (+61 3) 9035 7307

E-mail: imagetechliang@gmail.com

Abstract

Brain network modularity analysis has attracted increasing interest due to its capability in measuring the level of integration and segregation across subnetworks. Most studies have focused on extracting modules at a single level, although brain network modules are known to be organized in a hierarchical manner. A few techniques have been developed to extract hierarchical modularity in human functional brain networks using resting-state functional MRI data; however, the focus of those methods is binary networks produced by applying arbitrary thresholds of correlation coefficients to the connectivity matrices. In this study, we propose a new multi-subject spectral clustering technique, called Group-level Network Hierarchical Clustering (**GNetHiClus**), to extract the hierarchical structure of the functional network based on full weighted connectivity information. The most reliable results of hierarchical clustering are then estimated using a bootstrap aggregation algorithm. Specifically, we employ a voting-based ensemble method, i.e. majority voting; random subsamples with replacement are created for clustering brain regions, which are further aggregated to select the most reliable clustering results. The proposed method is evaluated over a range of group sample sizes, based on resting-state fMRI data from the Human Connectome Project. Our results show that **GNetHiClus** can extract relatively consistent hierarchical network structures across a range of sample size investigated. In addition, the results demonstrate that **GNetHiClus** can hierarchically cluster brain functional networks into specialized subnetworks from upper-to-lower level, including the high-level cognitive and the low-level perceptual networks. Conversely, from lower-to-upper level, information processed by specialized lower-level subnetworks are integrated into upper-level for achieving optimal efficiency for brain functional communications. Importantly, these findings are consistent with the concept of network

segregation and integration, suggesting that the proposed technique can be helpful to promote the understanding of brain network from a hierarchical point of view.

Key words: functional connectivity, spectral clustering, hierarchical clustering, bootstrapping,

INTRODUCTION

Modularity of brain networks provides selective adaptability, which has been demonstrated to play a key role in developmental optimization of the human brain (Meunier et al., 2009a). Hence, the detection of such community structures within brain networks, namely communities or modules, has attracted increasing interest (Meunier et al., 2009b, Ferrarini et al., 2009). Methods have been proposed to seek the optimal modules for a variety of complex networks (i.e. not limited to brain networks); a fundamental characteristic of such "modular" system is that nodes within modules are densely connected, whereas cross connections between modules are sparser (Newman, 2006, Newman and Girvan, 2004).

Importantly, Simon proposed that most complex systems are organized in a *hierarchical* manner, introducing the notion of "nearly-decomposable systems" (Simon, 1962), which has been well-accepted as fundamental for cognitive and computational neuroscience. In a stricter sense, a system is decomposable if its function can be decomposed to the sum of the independent functions of its parts. Furthermore, Simon suggested that hierarchies reduce the complexity of systems, which supports the feature of modularity. In this regard, a module (or a subsystem) can be considered as a self-enclosed unit that works almost independently, regardless of the changes that occur in other modules. Human brain network is an instantiation of such a hierarchically decomposable system.

Hierarchical modular networks

Previous studies support the concept that a brain functional network has an intrinsic hierarchical structure (Moretti and Munoz, 2013). However, most previous studies focused on studying modularity at a single level of the community structure, without mapping the properties or functions of the sub-modular communities at other hierarchical levels (Chen et al., 2008, Meunier

et al., 2009a). Extracting hierarchical structures from the brain network should help gain deeper insights and advance our understanding of brain organization from a network point of view.

Weighted vs. binary networks

There have been few studies developed to extract the hierarchical sub-networks. A recent study investigated the human functional brain networks at several hierarchical levels by applying a method for extracting hierarchical sub-networks (Meunier et al., 2009b). In another study, an approach was proposed to extract hierarchical functional modularity using an unbiased clustering coefficient (Ferrarini et al., 2009). Hierarchical functional modularity was also investigated in two more recent studies (Bassett et al., 2010, Power et al., 2011). Notably, all these studies require setting an arbitrary threshold for the correlation coefficient for measuring functional connectivity strength; different thresholds would unfavorably lead to distinct clustering outcomes. Furthermore, although binary networks obtained by applying arbitrary thresholds remain the most common approach employed for network analysis, weighted networks are increasingly recognized as they carry continuously characterization of brain connectivity (Bassett and Bullmore, 2016). Applying arbitrary thresholds could impose a detrimental effect on the subsequent network analyses (Garrison et al., 2015); a binarized connectivity matrix that discards putative connectivity strength might further deviate network measures from realistic biological connectivity, leading to compromised network analysis results.

Group-level vs individual-level networks

In general, functional networks are analyzed at either individual- or group-level. While the former could be important for some applications, such as subject-specific treatment (so-called precision medicine), its use has been limited due mainly to the relatively low signal-to-noise ratio

of fMRI data. Therefore, group-level network analysis has been most commonly employed. Brain functional networks at group-level are of great interest regarding probing the mechanism of complex brain function, and how networks change across disease condition and mental states. Group-level analyses have been mostly performed via the following ways: (a) direct averaging of individual-level networks across the group to obtain a single representative network for the group (Achard et al., 2006, Liang et al., 2014); or (b) estimating group-level networks by accounting for inter-subject variability with machine learning techniques (Varoquaux et al., 2010, Ng et al., 2013, Liang et al., 2016, Liang et al., 2017). Despite the popularity of the former approach, it fails to consider the variation among individual subjects. Thus, the latter studies advocate the incorporation of individual-level constraint to increase their robustness.

In this study, our objective is to robustly identify functional subnetworks of multiple hierarchical levels, directly from full weighted networks without filtering networks using arbitrary thresholds. To achieve this aim, we propose a novel multi-subject spectral clustering method in conjunction with a bootstrap ensemble learning technique, called Group-level Network Hierarchical Clustering (**GNetHiClus**). Further, the performance of **GNetHiClus** is assessed in terms of robustness and reproducibility based on resting-state fMRI data downloaded from the Human Connectome Project (http://www.humanconnectome.org, HCP).

MATERIALS AND METHODS

Motivation for developing GNetHiClus

There have been a variety of clustering algorithms available, of which the spectral clustering approach is very useful in hard, nonconvex clustering problems (Donath and Hoffman, 1973). Spectral clustering views the data clustering as a graph partitioning problem without relying on

any assumption on the form of data clustering. As such, the clustering results obtained by spectral clustering generally are more accurate than other approaches. Furthermore, spectral clustering can be easily implemented by applying linear algebra methods. Overall, therefore, spectral clustering provides a very efficient approach for clustering.

For conventional spectral clustering, *k*-means clustering is further applied to the eigenvectors obtained with spectral clustering, in order to determine the correct number of clusters. However, *k*-means clustering could be sensitive to initial conditions; subsequent analyses might be unfavorably affected by such uncertainty. Furthermore, such standard spectral clustering approaches are limited to extracting modularity at one particular level while ignoring hierarchical network topology.

To address the abovementioned limitations, we propose a hierarchical spectral clustering approach based on recursive bi-clustering. Specifically, subnetworks at the next level are obtained by subdividing each subnetwork at the current level, thereby providing detailed hierarchical network topology across multiple levels. Importantly, each bi-clustering process is exclusively based on spectral clustering, without being subject to the uncertainty issues intrinsic to k-means clustering.

In this study, we extend the multi-view spectral clustering technique (Kumar et al., 2011) to a multi-subject scenario, which could effectively integrate useful inter-subject information from every individual subject within a group via regularization, thereby achieving more reliable clustering results. By combining the hierarchical bi-clustering and multi-view spectral clustering techniques, we propose the ***GNetHiClus*** method to identify functional subnetworks at hierarchical-level by sharing individual-network information across subjects.

The spectral clustering technique

Generally, spectral clustering is implemented as follows:

(1) Adjacency-matrix: For a given set of data points $x_1, \ldots, x_n$, a similarity graph $G = (V_t, E)$ can be employed to represent the data, with $V_t = \{v_1, \ldots, v_n\}$ and *E* representing vertices and edges respectively. The adjacency-matrix $A = (a_{i,j})_{i,j=1,\ldots,n}$ of the graph is employed to characterize the similarity between vertices v_i and v_j, with a nonnegative weight a_{ij} .

(2) Normalized adjacency-matrix (Chung, 1997)

$$N_1 = D^{-1/2} A D^{-1/2} \quad (1)$$

Where the degree-matrix *D* is defined as diagonal matrix with node degrees $d_1, \ldots, d_n$ on the diagonal. To make sure normalized adjacency matrix is symmetric, we let $N = (N_1 + {N_1}^T)/2$. Spectral clustering algorithm solves the following optimization problem for the normalized adjacency-matrix *N*:

$$\max_{U \in R^{n \times k}} tr(U^T N U), \text{ s.t. } U^T U = I,$$

where *tr* represents the trace of a matrix.

(3) Compute *k* eigenvectors corresponding to the *k* largest eigenvalues. Specifically, here we consider *k*=2 (with two eigenvectors u_1 and u_2) because our proposed approach relies on iterative bi-clustering. In particular, the second largest eigenvector u_2 is also called a Fiedler vector, which can be used to divide its elements into two clusters based on their associated signs (Fiedler, 1973), i.e. a cluster corresponding to the data points with elements of "+" sign and another cluster with those that have "-" sign (see Figure 1 for an illustrative example).

The original multi-view spectral clustering approach

Basically, a multi-view spectral clustering approach can be considered as a way to extract information from different data representations (such as multi-modality or multi-subject data) to achieve more accurate clustering results. While multiple views of data might be available in many scenarios, such complementary information cannot be fully utilized without an appropriate multi-view approach. To fully utilize such complementary information (i.e. information across subjects in our study), a co-regularized multi-view spectral clustering was proposed by Kumar and colleagues (Kumar et al., 2011); they demonstrated the advantages of their approach over other existing techniques for data clustering. In that study, a centroid-based co-regularization was proposed for regularizing each view-specific set of eigenvectors $U^{(v)}$ ($v=1,2,\ldots,m$) towards a common centroid $U^{(*)}$, with m representing the total number of views. The objective function is formulated as:

$$\max_{U^{(1)},U^{(2)},\ldots,U^{(m)},U^{*}\in R^{n\times k}} \sum_{v=1}^{m}[tr(U^{(v)^T}N^{(v)}U^{(v)}) + \lambda_v tr(U^{(v)}U^{(v)^T}U^{*}U^{*^T})], \quad (2)$$

$$\text{s.t. } U^{(v)^T}U^{(v)} = I, \forall 1 \le v \le m, U^{*^T}U^{*} = I.$$

This objective function essentially tries to estimate consensus eigenvectors $U^{(*)}$ from m views through regularization; each regularization term is weighted by a weighting parameter λ_v that reflects the importance of view v.

The objective function can be solved in an alternating way that optimize one single view-specific eigenvector $U^{(v)}$ at a time, while fixing all other variables. Thus, the objective function for optimizing $U^{(v)}$ for view v is reformulated as follows:

$$\max_{U^{(v)}\in R^{n\times k}} tr(U^{(v)^T}N^{(v)}U^{(v)}) + \lambda_v tr(U^{(v)}U^{(v)^T}U^{*}U^{*^T}),\ \text{s.t. } U^{(v)^T}U^{(v)} = I \quad (3)$$

Eq. (3) can be written as follows:

$$\max_{U^{(v)} \in R^{n \times k}} tr(U^{(v)^T}(N^{(v)} + \lambda_v U^* U^{*^T})U^{(v)}), \text{ s.t. } U^{(v)^T} U^{(v)} = I \quad (4)$$

This provides a standard spectral clustering objective for $U^{(v)}$ with a modified normalized adjacency-matrix $N^{(v)} + \lambda_v U^* U^{*^T}$.

Next, consensus $U^{(*)}$ is optimized by keeping all view-specific eigenvectors $U^{(v)}$ fixed. With Eq. [2], $U^{(*)}$ can be obtained by solving the following equation:

$$\max_{U^* \in R^{n \times k}} \sum_v \lambda_v tr(U^{(v)} U^{(v)^T} U^* U^{*^T}), \text{ s.t. } U^{(*)^T} U^{(*)} = I \quad (5)$$

The cyclic property of matrix traces (i.e. for square matrices A, B and C, *Tr(ABC)=Tr(BCA)=Tr(CAB)*) is then applied to reformulate Eq. [5] as a standard spectral clustering objective for $U^{(*)}$ as follows:

$$\max_{U^* \in R^{n \times k}} tr(U^{*^{(T)}}(\sum_v \lambda_v (U^{(v)} U^{(v)^T}))U^*), \text{ s.t. } U^{(*)^T} U^{(*)} = I \quad (6)$$

with a modified normalized adjacency-matrix $N_m = \sum_v \lambda_v (U^{(v)} U^{(v)^T})$.

Eq. [6] could be reformulated as $\max_{U^* \in R^{n \times k}} tr(U^{*^{(T)}} U^*)$, $\text{s.t. } U^{(*)^T} U^{(*)} = I$; the solution to this equation can be obtained by using the standard spectral clustering approach (Ng et al., 2002), given the provided standard spectral clustering objective for $U^{(v)}$ $(v = 1,2, \dots, m)$ and $U^{(*)}$. In practice, the multi-view spectral clustering approach is iteratively implemented; the clustering procedure stops when the difference in value of objective function between consecutive iterations falls below a relatively low threshold ($\varepsilon = 10^{-4}$) (Kumar et al., 2011), suggesting that the optimal solution is achieved.

The proposed GNetHiClus approach

GNetHiClus consists of 2 parts (part *I* and *II*) - A flowchart is shown in Figure 2:

(I) The <u>multi-subject spectral clustering</u> described above is used to estimate a consensus (group-level) eigenvector of normalized adjacency-matrices and consistent individual-level eigenvectors and eigenvalues across the group. It includes the following steps:

(a) Using BOLD fMRI data to generate an adjacency-matrix $A^{(v)}$ for a subject *v* (*v=1,...,m*), where *m* is the number of subjects within the group.

(b) Calculating normalized adjacency-matrix ${N_1}^{(v)} = {D^{(v)}}^{-1/2} A^{(v)} {D^{(v)}}^{-1/2}$, *D*: degree-matrix. $N = (N_1 + {N_1}^T)/2$.

(c) Calculating eigenvectors $U^{(v)}$ by eigenvalue-decomposition of $N^{(v)}$. In particular, we are interested in the second eigenvalue and eigenvector (see (h) below).

(d) Updating group consensus U^G : solving $\max_{U^G \in R^{n \times k}} tr\{{U^G}^T (\sum_v \lambda_v (U^{(v)} {U^{(v)}}^T)) U^G\}$, $\text{s.t.}\, {U^G}^T U^G = I$, by eigenvalue-decomposition on $\sum_v \lambda_v (U^{(v)} {U^{(v)}}^T)$, with $U^{(v)}$ from (c) for first iteration, *n:* number of nodes, *k:* number of clusters, λ_v: weight (i.e. the 'importance' of subject *v*, $\lambda_v = 1 - D$, with *D* representing disagreement between subjects (views) (see Kumar et al., 2011 for the calculation of *D (Eq. 2)*); Note: *k*=2 due to bi-clustering in our study, therefore *k*=2 for GNetHiClus).

(e) Updating $U^{(v)}$: solving $\max_{U^{(v)} \in R^{n \times k}} tr\{{U^{(v)}}^T (N^{(v)} + \lambda_v U^G {U^G}^T) U^{(v)}\}$, $\text{s.t.}\, {U^{(v)}}^T U^{(v)} = I$, by eigenvalue-decomposition on $N^{(v)} + \lambda_v U^G {U^G}^T$, with all other $U^{(v)}$ and U^G fixed.

(f) Updating $U^{(v)}$ and U^G iteratively via (d) and (e) until convergence (Kumar et al., 2011), yielding final estimates of U^G, $U^{(v)}$ and $EV^{(v)}$ (i.e. eigenvalues).

(II) <u>The hierarchical-clustering</u> is used to hierarchically divide the networks (or subnetworks) into 2 clusters downstream from the current level using U^G, $U^{(v)}$ and $EV^{(v)}$ from (*I*).

*(**g**)* For each cluster, if the median of Fiedler eigenvalues of all individual subjects across the group is positive (i.e. more than half of the subjects have a positive second largest eigenvalue), continue to step (**h**); otherwise, stop performing further clustering;

(**h**) The nodes are assigned into 2 different clusters based on the signs of the Fiedler vectors (i.e. "+" or "-").

(i) Furthermore, since brain subnetworks tend to be bilateral (Tyszka et al., 2011, Meunier et al., 2009b), homotopic brain regions are forced to be present in the same subnetworks to which the homotopic regions are more likely belonging, which is determined as follows:

(1) For region i (and j), whether i (and j) is identified in cluster A or cluster B is firstly determined at individual-level, i.e. total numbers of subjects that vote for region i (and j) to be in clusters A and B are counted;

(2) Then, for region i (and j), the magnitudes of eigenvector entries corresponding to region i are summed across those subjects identifying i (and j) to be in the cluster A at individual-level, i.e. $S_A(i)$ and $S_A(j)$ are computed;

(3) Similarly, for region i (and j), the magnitudes of eigenvector entries corresponding to region i are summed across those subjects identifying i (and j) to be in the cluster B at individual-level, i.e. $S_B(i)$ and $S_B(j)$ are computed;

(4) Finally, if $S_A(i) + S_A(j) > S_B(i) + S_B(j)$, then the (i,j) pair is assigned to cluster A, otherwise, it is assigned to cluster B.

(**j**) Two new clusters obtained at the current-level are fed into (*I*) recursively, until all clusters cannot be divided based on the criteria in (g).

Matlab code to perform the proposed method can be downloaded from https://www.florey.edu.au/science-research/scientific-services-facilities/human-mri/imaging-software.[1]

MRI Data Acquisition

Resting-state FIX-denoised (Salimi-Khorshidi et al., 2014) fMRI data of 133 subjects (n=133) were downloaded from the ConnectomeDB (https://db.humanconnectome.org). Data of 1200 volumes had been acquired in a Siemens 3T Connectome Skyra system, using a gradient-echo slice-accelerated multiband EPI sequence at 2 mm isotropic resolution, with TR/TE = 720/33.1 ms. See (Glasser et al., 2013; Van Essen et al., 2013) for HCP data acquisition details.

Data Analysis

Network construction

Networks are constructed as follows: (i) the automated anatomical labeling *(*AAL) template (Tzourio-Mazoyer et al., 2002) was used to parcellate the whole-brain into 90 regions (cerebellum was excluded); (ii) region-wise mean time-series were calculated across all voxels within each region (size: 90×1200); (iii) individual-level functional connectivity matrix (size: 90×90) was constructed from region-wise mean time-series of each subject using Pearson-correlation.

Hierarchical clustering results: statistical modeling and analyses

GNetHiClus is implemented with the following two-level analysis. Firstly, the first-level analysis for selecting most representative clustering results across bootstrap datasets. Secondly, the second-

[1] *Note to the Editor and reviewers*: Please note that this code will be uploaded on acceptance of a final version of the manuscript.

level analysis for identifying the final clustering results with the highest probability across repetitions of the first-level analysis.

(i) Bootstrapping: since ***GNetHiClus*** is implemented across all subjects, only a single group outcome is obtained, to which regular statistical analyses could not be applied. To address this issue, the bootstrap method relying on random subsampling with replacement was employed. For a given number of total subjects (i.e. a subset of the maximum 133 subjects, which was considered to investigate the effect of sample size), random subsampling was implemented using a fixed ratio of ~60% with a variable subsampling size (i.e. the ratio between the number of randomly-subsampled subjects and the total number of subjects in the pool): 75/125, 70/117,65/108,60/100,55/92, and 50/83. As an example, for the case of 75/125, each subsampled dataset was obtained by randomly selecting 75 subjects out of a total of 125 subjects; this procedure was then repeated 100 times to generate 100 subsampled datasets. We sought to identify the optimal implementation strategies for the bootstrapping among all these 6 cases, i.e. we aim to determine the optimal subsamples (and total subjects) that can achieve robust hierarchical clustering results. As more reliable results are expected when using larger sample sizes, the clustering results of 80/133 are employed as a 'ground-truth' for evaluating the other results with smaller sample sizes.

(ii) Extraction of the most representative clustering results for each of the 6 cases: (a) **GNetHiClus** was applied to each of the 100 bootstrap subsamples to extract hierarchical subnetworks; (b) normalized mutual information (NMI) (Fred and Jain, 2003) was calculated between each subsample and the remaining 99 subsamples, yielding a 100×99 matrix of NMI values; (c) the 99 NMI values were averaged, yielding a vector of 100×1 mean NMI (mNMI) values; (d) the subsample having the highest mNMI was selected from the vector of 100 mNMIs; (e) hierarchical

subnetworks that produced the highest mNMI were designated as the most reliable clustering results. The reasons for choosing NMI to evaluate the proposed method are as follows: (a) It is a good measure for determining the performance of clustering; and (b) NMI can be used to compare clustering results having different number of clusters (Danon et al., 2005). In general, the higher NMI values indicate the more accurate clustering results are obtained (NMI$\in$ [0,1], with NMI=1 indicating perfect clustering results.

(iii) Measurement of probability of clusters: (a) the step (ii) was repeated 100 times to obtain 100 groups of clusters (i.e. 10,000 bootstraps), of which, each group was expressed as a 90×90 matrix and all members of each cluster was denoted with a unique number; (b) for each of the 100 groups (i.e. 100 matrices of size 90×90), we counted the total number of occurrences of each cluster, $T_{cluster}$, by searching over all clusters and all groups; (c) for each of the 100 groups, the total number of occurrences of all clusters, T_{all}, belonging to the group was calculated; (d) The group with the maximum T_{all} was then selected as the optimal group, which yielded the clustering results with the highest overall probability; (e) those clusters corresponding to the identified optimal group were designated as the final clustering results; (f) for the obtained clustering results, the probability of each cluster, p, was calculated as p= $T_{cluster}/100$.

RESULTS

Our results show that **GNetHiClus** extracts 13 functional subnetworks (the green clusters at the bottom level) from resting-state HCP fMRI data for subsample/sample sizes of 75/125 (Figure 3). Importantly, the results suggest that **GNetHiClus** can automatically organize the whole brain functional networks into a hierarchical 'tree' structure where each branch represents a well-established functional subnetwork of the human brain. As shown in Figure 3, the whole-brain network is first divided into *low-level perceptual* and *high-order cognitive* networks, from which

well-known resting-state brain networks are hierarchically clustered; these subnetworks include visual, auditory/somatomotor, default-mode, and attention networks.

Specifically,13 functional subnetworks extracted at the finest levels, i.e. 4^{th}&5^{th} levels in Figure 3, are shown in Figure 4. The nodes of these undividable subnetworks are displayed using the AAL atlas. To facilitate interpretation, the undividable subnetworks are aggregated (but colored differently to differentiate the clusters) into 4 well-known resting-state networks, i.e. visual, auditory/somatomotor, default-mode and attention networks. Table 1 summarizes the brain nodes of each cluster for the case of using subsamples/samples = 75/125,70/117, 60/100 & 55/92 showing high correspondence between those clustered brain regions with their roles known in human brain functions.

As expected, increasing subsample/sample sizes improved clustering results. For 70/117 and 75/125, the clustering results were consistent with 80/133, as shown in Figure 5(a), also achieving more persistent probabilities of all clusters (Figure 6 (e) & (f)) than all other cases (Figure 6 (a), (b), (c) &(d)). When lower subsampling/sampling sizes, i.e. 65/108, slightly different clustering results were obtained: the bilateral DCG, which were classified into auditory/somatomotor networks for 80/133, were erroneously identified as nodes of attention networks (Figure 5(b)). While clustering results of 60/100 and 55/92 were also consistent with 80/133, these probabilities are not persistent across all clusters, i.e. some clusters have very low probabilities (see Figure 6(b) & (c)). As expected, when using the lowest subsampling/sampling size of 50/83, in addition to the common difference observed in 65/108, one of the subnetworks (i.e. cluster 26 in Figure 3) within DMN was further divided into 2 clusters, showing apparent deviation from the ground truth of 80/133 (see Figure 5(c); cluster 1: ORBinf.L, ORBinf.R, ITG.L & ITG.R; cluster 2: MTG.L, MTG.R, TPOsup.L, TPOsup.R, TPOmid.L & TPOsup.R).

With the clustering results from 80/133 as ground truth, overall high NMI values are obtained. For clusters having the highest overall probability among all 100 repetitions of each case, their NMI values were 0.9662, 1, 1, 0.9806 and 1, 1 for sampling sizes of 50/83, 55/92, 60/100, 65/108, 70/117, and 75/125, respectively. This demonstrates that **GNetHiClus** achieves clustering outcomes with fairly high accuracy (as indicated by high NMI values) for most of the clusters even with relatively low subsampling/sampling sizes, i.e. 50/83.

DISCUSSION

In this study, a multi-subject hierarchical spectral clustering method, **GNetHiClus**, has been proposed. Specifically, this is a recursive bi-clustering approach, where brain nodes are hierarchically bi-clustered into subnetworks until stopping criteria are met. In this way, functional hierarchical network structure of the human brain can be reconstructed from resting-state fMRI data. A bootstrap ensemble learning technique is adopted to compute the most representative functional hierarchical structure via repeatedly applying **GNetHiClus** on the bootstrap datasets (i.e. a subset of randomly selected individuals). The performance of the proposed method in clustering brain networks is evaluated by using the publicly available HCP data; the consistency of our results with the concept of low-level perceptual and high-order cognitive networks (Shang et al., 2014, Mottron et al., 2006) along with hierarchical subnetworks (such as visual, somatosensory, DMN, and attention networks) demonstrate that the proposed method can achieve biologically-reasonable hierarchical structures that characterize specialized functional networks. The main novelties of **GNetHiClus** are discussed point-by-point in the following sections:

(i) Avoiding uncertainty of choosing arbitrary thresholds

Previous network clustering approaches commonly rely on applying arbitrary thresholds to the correlation coefficients of inter-regional functional connectivity, with different thresholds possibly

leading to different network clustering outcomes (or modularity). Empirically, the computation of network modularity is highly dependent on network density, with higher modularity achieved by using lower network density; as an extreme case, network modularity analysis might not be practically feasible if no thresholds are applied (i.e. for fully connected networks, conventional network modularity might detect the whole brain network as a single modular). In contrast, **GNetHiClus** takes weighted-networks as the input without requiring arbitrary thresholds and binarizing the networks; it is rather immune to network density because it directly uses full networks for performing clustering, where per-edge connectivity strength is the main determinants to the outcome of network clustering. Therefore, **GNetHiClus** can exclude the uncertainty induced by the selection of threshold values, potentially providing a more robust and consistent approach for investigating brain networks. However, direct comparisons between GNetHiClus and the existing threshold-based techniques are beyond the scope of the current study.

(ii) Ensemble learning to reduce sensitivity to noise

Network clustering is prone to the influence of noise, particularly in resting-state functional connectivity where BOLD contrast is sensitive to noise; it is therefore not ideal to rely on a single clustering result. Aggregation of many estimators could reduce the effect of noise, leading to more accurate results. In this study, bootstrapping is employed to generate randomly subsampled datasets with replacement: we employed an ensemble learning approach that is analogous to a majority voting-based ensemble algorithm (Lam and Suen, 1997); it trains models through randomly selecting multiple sets of subsamples from the training datasets, and then aggregates the votes (i.e. clustering results) from different models to decide the final class of the test object. Specifically, **GNetHiClus** is implemented with two-level analysis, i.e. the first-level analysis for selecting most representative clustering results across 100 bootstrapping datasets and the second-

level analysis for identifying clustering results with highest-probability across first-level 100 repetitions. In contrast, previously methods have been mainly relying on obtaining average connectivity matrix from a group followed by the identification of (hierarchical) subnetworks. In particular, we proposed a novel and robust machine learning framework for investigating hierarchical networks, which can quantify the probability of extracting hierarchical functional modularity.

(iii) Uncovering hierarchical structure

While there is no direct ground truth available, the identified subnetworks of our hierarchical structure are overall consistent with resting-state networks extracted using other approaches, such as independent-component analysis (ICA) (Beckmann et al., 2005); note however that ICA cannot yield hierarchical network structure. Previous studies have shown that visual, sensorimotor, auditory, default mode, attention, executive-control, and subcortical networks are commonly detected from resting-state human brain using either BOLD or arterial spin labeling perfusion fMRI (Beckmann et al., 2005, Liang et al., 2012). Similarly, with **GNetHiClus**, visual, sensorimotor/auditory, default mode, attention networks are extracted. Of note, due to the differences in the fundamental algorithms, there are a few apparent differences in the subnetwork extraction between previous findings and our clustering results: using ICA, the sensorimotor and the auditory network are identified as a single cluster (Beckmann et al., 2005, Liang et al., 2012); using **GNetHiClus,** the attention, the executive control and the subcortical network are identified as a single cluster.

Note that we are not implying the proposed method is the only available approach to achieve hierarchical brain decomposition, but we described a novel approach to achieve this goal that has a number of important features.

Overall, the aim of this study is to recursively divide a large group of objects (i.e. brain regions in the current study) into relatively small groups that share certain similarities given the relationships (i.e. network connection strength) among all objects. This has been commonly perceived as community structure detection (or network modularity analysis), with which methods for analyzing network modularity have been developed (Newman, 2006, Newman and Girvan, 2004). These methods have been successfully employed for analyzing network modularity, but hierarchical network structure cannot be uncovered. Importantly, our method provides the capability of revealing hierarchical subnetworks across different levels, a goal that was also achieved in two previous studies (Meunier et al., 2009b, Ferrarini et al., 2009). However, direct comparisons between the proposed method and these two previous approaches were not conducted for the following reasons: (1) both previous studies focused on binary networks by setting arbitrary thresholds, instead of weighted networks in our study; (2) Ferrarini and colleagues employed partial correlations (Ferrarini et al., 2009), instead of full correlation as in our study.

Effect of sample size on group-level analysis

Given the use of bootstrapping approach, subsampling/sample size could be one of the most important factors that affect the final estimation of the clustering results. Our results have shown that reliable clustering results can be achieved with relatively high probability for subsampling/sample size of 70/117 and 75/125. While fully consistent results cannot be obtained with lower number of subsampling/sample size, i.e. 65/108, further inspection reveals that only one pair of brain regions are not desirably extracted into the right cluster. It should be noted that fully consistent clustering results have been also achieved for 60/100 and 55/92, albeit with a few clusters of low probability. Taken together, these clustering results suggest that the proposed method, GNetHiClus, can achieve satisfactory clustering outcomes (i.e. no more than a pair of

brain regions are incorrectly assigned) with 75/125, 70/117, 65/108, 60/100, and 55/92. In contrast, regarding 50/83, four pairs of brain regions have not been correctly clustered into right clusters, indicating its inferior performance in comparison to those clustering results obtained with larger subsample sizes/sample sizes. Further, among all extracted subnetworks, while visual subnetworks are the most reliable, auditory/somatomotor subnetworks are the least reliable ones, whose reliability cannot be consistently improved by increasing the subsampling/sampling sizes; further investigation is, therefore, warranted. Regardless, results have demonstrated that acceptable clustering results should still be achievable by using the proposed method, **GNetHiClus,** with reduced total number of subjects.

Use of the bilateral homotopic constraint

In **GNetHiClus**, homotopic brain regions are explicitly constrained to be clustered in the same subnetwork in order to minimize the noise effect (see also "Limitations" section below). A previous study has shown that spontaneous brain activity is highly correlated across homotopic regions between left and right hemispheres (Tyszka et al., 2011), which suggests that homotopic regions tend to be cooperative with each other to achieve optimal brain function. Interestingly, such a bilateral symmetric property was also shown in both healthy adults and patients with complete agenesis of corpus callosum (Tyszka et al., 2011). This supports the plausibility of the bilateral homotopic constraint adopted in **GNetHiClus**.

Limitations

In this study, **GNetHiClus** is evaluated by using a relatively large number of subjects, based on the high-quality HCP MRI datasets. Our results have shown that a total number of ~90 subjects are required to achieve acceptable clustering results, which might not be readily achievable for some clinical studies, due to the relatively small number of patients often collected. However, such

a sample size should be feasible for multi-site studies that collect relatively large cohorts, which is becoming increasingly common in the field.

The use of the bootstrapping technique in **GNetHiClus** imposes a computational demand, discouraging its application to high spatial-resolution parcellation schemes (Glasser et al., 2016) – or alternatively requiring the access to high performance computing. We acknowledge that low-resolution AAL parcellation used in the current study also has limitations. However, the parcellation was selected however selected primarily based on the following reasons: (1) it is a commonly used parcellation template; (2) the empirical evidence of hierarchical modularity is likely to be more accessible; (3) finer parcellation might be more informative, but it dramatically increases the computational burden.

For healthy subjects, the homotopic constraint (Tyszka et al., 2011) can be employed for achieving more reliable clustering results by removing uncertainty in assigning brain regions into specific clusters. However, it is not clear if this constraint is still appropriate for patients with abnormal brain functions. To deal with such scenarios, further work is warranted to develop an alternative reliable approach for extracting subnetworks from group of patients with abnormal brain function without having to explicitly rely on a homotopic constraint. Future studies on the validity of the bilaterally homotopic constraint might provide important information on understanding the mechanism for maintaining normal brain function.

CONCLUSION

In this study, we proposed a novel approach, **GNetHiClus**, for hierarchically clustering the brain network into subnetworks, without relying on applying arbitrary thresholds to cross-coefficients. Importantly, rather than performing clustering at individual-level, we employed a multi-subject approach, sharing information across subjects. Our results show that **GNetHiClus** can

hierarchically cluster brain functional network into specialized subnetworks that fulfill specialized tasks; conversely, information processed by specialized lower-level subnetworks are integrated into upper-level for achieving optimal efficiency. Our findings are consistent with the concept of network segregation and integration. This proposed technique should promote the understanding of brain network from a hierarchical point of view.

ACKNOWLEDGEMENTS

We are grateful to the National Health and Medical Research Council (NHMRC) of Australia, the Australian Research Council (ARC), and the Victorian Government's Operational Infrastructure Support Program for their support. Data were provided in part by the Human Connectome Project, WU-Minn Consortium (Principal Investigators: David Van Essen and Kamil Ugurbil; 1U54MH091657) funded by the 16 NIH Institutes and Centers that support the NIH Blueprint for Neuroscience Research; and by the McDonnell Center for Systems Neuroscience at Washington University.

DISCLOSURE STATEMENT

No competing financial interests exist.

REFERENCES

ACHARD, S., SALVADOR, R., WHITCHER, B., SUCKLING, J. & BULLMORE, E. 2006. A resilient, low-frequency, small-world human brain functional network with highly connected association cortical hubs. *J Neurosci,* 26**,** 63-72.

BASSETT, D. S. & BULLMORE, E. T. 2016. Small-World Brain Networks Revisited. *Neuroscientist*.

BASSETT, D. S., GREENFIELD, D. L., MEYER-LINDENBERG, A., WEINBERGER, D. R., MOORE, S. W. & BULLMORE, E. T. 2010. Efficient physical embedding of topologically complex information processing networks in brains and computer circuits. *PLoS Comput Biol,* 6**,** e1000748.

BECKMANN, C. F., DELUCA, M., DEVLIN, J. T. & SMITH, S. M. 2005. Investigations into resting-state connectivity using independent component analysis. *Philos Trans R Soc Lond B Biol Sci,* 360**,** 1001-13.

CHEN, Z. J., HE, Y., ROSA-NETO, P., GERMANN, J. & EVANS, A. C. 2008. Revealing modular architecture of human brain structural networks by using cortical thickness from MRI. *Cereb Cortex,* 18**,** 2374-81.

CHUNG, F. 1997. Spectral graph theory. *Conference Board of the Mathematical Sciences.* Washington.

DANON, L., DIAZ-GUILERA, A., DUCH, J. & ARENAS, A. 2005. Comparing community structure identification. *Journal of Statistical Mechanics-Theory and Experiment*.

DONATH, W. E. & HOFFMAN, A. J. 1973. Lower Bounds for Partitioning of Graphs. *Ibm Journal of Research and Development,* 17**,** 420-425.

FERRARINI, L., VEER, I. M., BAERENDS, E., VAN TOL, M. J., RENKEN, R. J., VAN DER WEE, N. J., VELTMAN, D. J., ALEMAN, A., ZITMAN, F. G., PENNINX, B. W., VAN BUCHEM, M. A., REIBER, J. H., ROMBOUTS, S. A. & MILLES, J. 2009. Hierarchical functional modularity in the resting-state human brain. *Hum Brain Mapp,* 30**,** 2220-31.

FIEDLER, M. 1973. Algebraic Connectivity of Graphs. *Czechoslovak Mathematical Journal,* 23**,** 298-305.

FRED, A. & JAIN, A. Robust data clustering. 2003 IEEE Computer Society Conference on Computer Vision and Pattern Recognition, 6/18/03 2003 Madison, WI, United States.

GARRISON, K. A., SCHEINOST, D., FINN, E. S., SHEN, X. & CONSTABLE, R. T. 2015. The (in)stability of functional brain network measures across thresholds. *Neuroimage,* 118**,** 651-61.

GLASSER, M. F., COALSON, T. S., ROBINSON, E. C., HACKER, C. D., HARWELL, J., YACOUB, E., UGURBIL, K., ANDERSSON, J., BECKMANN, C. F., JENKINSON, M., SMITH, S. M. & VAN ESSEN, D. C. 2016. A multi-modal parcellation of human cerebral cortex. *Nature,* 536**,** 171-178.

KUMAR, A., P., R. & DAUME III, H. Co-regularized multi-view spectral clustering. Proceedings of the 24th International Conference on Neural Information Processing Systems, 2011. 1413-21.

LAM, L. & SUEN, C. Y. 1997. Application of majority voting to pattern recognition: An analysis of its behavior and performance. *Ieee Transactions on Systems Man and Cybernetics Part a-Systems and Humans,* 27**,** 553-568.

LIANG, X., CONNELLY, A. & CALAMANTE, F. 2014. Graph analysis of resting-state ASL perfusion MRI data: nonlinear correlations among CBF and network metrics. *Neuroimage,* 87**,** 265-75.

LIANG, X., CONNELLY, A. & CALAMANTE, F. 2016. A novel joint sparse partial correlation method for estimating group functional networks. *Hum Brain Mapp,* 37**,** 1162-77.

LIANG, X., TOURNIER, J. D., MASTERTON, R., CONNELLY, A. & CALAMANTE, F. 2012. A k-space sharing 3D GRASE pseudocontinuous ASL method for whole-brain resting-state functional connectivity. *International Journal of Imaging Systems and Technology,* 22**,** 37-43.

LIANG, X., VAUGHAN, D. N., CONNELLY, A. & CALAMANTE, F. 2017. A Novel Group-Fused Sparse Partial Correlation Method for Simultaneous Estimation of Functional Networks in Group Comparison Studies. *Brain Topogr*.

MEUNIER, D., ACHARD, S., MORCOM, A. & BULLMORE, E. 2009a. Age-related changes in modular organization of human brain functional networks. *Neuroimage,* 44**,** 715-23.

MEUNIER, D., LAMBIOTTE, R., FORNITO, A., ERSCHE, K. D. & BULLMORE, E. T. 2009b. Hierarchical modularity in human brain functional networks. *Front Neuroinform,* 3**,** 37.

MORETTI, P. & MUNOZ, M. A. 2013. Griffiths phases and the stretching of criticality in brain networks. *Nature Communications,* 4.

MOTTRON, L., DAWSON, M., SOULIERES, I., HUBERT, B. & BURACK, J. 2006. Enhanced perceptual functioning in autism: an update, and eight principles of autistic perception. *J Autism Dev Disord,* 36**,** 27-43.

NEWMAN, M. E. J. 2006. Modularity and community structure in networks. *Proceedings of the National Academy of Sciences of the United States of America,* 103**,** 8577-8582.

NEWMAN, M. E. J. & GIRVAN, M. 2004. Finding and evaluating community structure in networks. *Physical Review E,* 69.

NG, A. Y., JORDAN, M. I. & WEISS, Y. 2002. On spectral clustering: Analysis and an algorithm. *Advances in Neural Information Processing Systems 14, Vols 1 and 2,* 14**,** 849-856.

NG, B., VAROQUAUX, G., POLINE, J. B. & THIRION, B. 2013. A novel sparse group Gaussian graphical model for functional connectivity estimation. *Inf Process Med Imaging,* 23**,** 256-67.

POWER, J. D., COHEN, A. L., NELSON, S. M., WIG, G. S., BARNES, K. A., CHURCH, J. A., VOGEL, A. C., LAUMANN, T. O., MIEZIN, F. M., SCHLAGGAR, B. L. & PETERSEN, S. E. 2011. Functional network organization of the human brain. *Neuron,* 72**,** 665-78.

SALIMI-KHORSHIDI, G., DOUAUD, G., BECKMANN, C. F., GLASSER, M. F., GRIFFANTI, L. & SMITH, S. M. 2014. Automatic denoising of functional MRI data: combining independent component analysis and hierarchical fusion of classifiers. *Neuroimage,* 90**,** 449-68.

SHANG, J., LUI, S., MENG, Y., ZHU, H., QIU, C., GONG, Q., LIAO, W. & ZHANG, W. 2014. Alterations in low-level perceptual networks related to clinical severity in PTSD after an earthquake: a resting-state fMRI study. *PLoS One,* 9**,** e96834.

SIMON, H. 1962. The architecture of complexity. *Proc. Am. Philos, Soc.,* 106**,** 467-82.

TYSZKA, J. M., KENNEDY, D. P., ADOLPHS, R. & PAUL, L. K. 2011. Intact bilateral resting-state networks in the absence of the corpus callosum. *J Neurosci,* 31**,** 15154-62.

TZOURIO-MAZOYER, N., LANDEAU, B., PAPATHANASSIOU, D., CRIVELLO, F., ETARD, O., DELCROIX, N., MAZOYER, B. & JOLIOT, M. 2002. Automated anatomical labeling of activations in SPM using a macroscopic anatomical parcellation of the MNI MRI single-subject brain. *Neuroimage,* 15**,** 273-89.

VAROQUAUX, G., GRAMFORT, A., POLINE, J. B. & THIRION, B. 2010. Brain covariance selection: better individual functional models using population prior. *Advances in Neural Information Processing Systems,* 23**,** 2334-42.

FIGURE CAPTIONS

Figure 1: An illustrative example of the overall concept of spectral clustering. Given a normalized adjacency matrix with 4 nodes, Fiedler vector (i.e. the 2nd eigenvector derived from eigen-decomposition of the input matrix) can be employed to divide the original 4 nodes (1,2,3 & 4) into 2 clusters based on the positive and negative signs of the values of Fiedler vector. In this example, nodes 1 & 2 are classified into a cluster, and nodes 3 & 4 are assigned into another.

Figure 2: The workflow of **GNetHiClus** for extracting hierarchical functional subnetworks. The flowchart can be divided into 2 major parts, as grouped by 2 dashed boxes: (Left) Multi-subject spectral clustering (steps (a-f)); (Right) Hierarchical clustering (steps (g-j)). See Methods for the detailed description of each step and the definition of each symbol within the flowchart. Note: this procedure needs to be repeated for a certain number of times (e.g. 100 times in this study) to realize ensemble learning through bootstrapping.

Figure 3: Results of hierarchically-clustered subnetworks using **GNetHiClus**, for the case of using 75/125 subsample/sample size. From upper-to-lower level of the figure, the brain network is hierarchically subdivided into 2 clusters until stopping criterion is met. Each circle indicates a cluster, with green ones represent the final clusters and blue ones represent clusters at intermediate stage. At the second-level (i.e. following the first division), the result show that **GNetHiClus** subdivides the whole brain functional network into 2 meaningful major subnetworks, one corresponds to the low-level perceptual network (cluster #2) and the other one corresponds to the higher-order cognitive network (cluster #3). At the third-level, the result shown that the visual- and the somato-motor-network (SMN) are separated from low-level perceptual network, while the default-mode- (DMN) and the attention-network are divided by the high-order cognitive network. These functional specialized subnetworks can be further divided into subnetworks at finer levels

(4^{th} and 5^{th}) to fulfill specialized tasks. Likewise, from lower-to-upper level, the outcome of hierarchical structure can be used to conversely integrate subnetworks into whole-brain network. Also refer to Figure 4 and Table 1 for a detailed description of the constituents of each subnetwork.

Figure 4: Visualization of all functional subnetworks at the finest levels, i.e. 4^{th} and 5^{th} levels in Figure 3. The whole-brain network is divided into 4 meaningful resting-state functional networks, i.e. visual, auditory/somatomotor, default-mode and attention networks, which are shown in Figure 3 (a), (b), (c) & (d), respectively. In each subfigure, those colored circles compose the current focused network. The 4 resting-state networks can be further partitioned into finer subnetworks (until indivisible), with each subnetwork represented in a different color. See Table 1 for definition of node acronyms. Note: We just show the relevant part of the tree in each subfigure (see Figure 3 for the full tree), with each colored circle corresponding to a set of nodes with the same color mapped onto the brain; as an example, Figure 4(a) focuses on visual network, where yellow circle represents medial visual network and green circle represents lateral visual network.

Figure 5: Results of **GNetHiClus** for different subsample and sample sizes. Visual network, SMN, DMN and attention network at the third level (see Figure 3) are displayed with nodes mapped onto the AAL template. In each of these 4 networks, the lowest-level indivisible subnetworks extracted are represented in different colors, with each color corresponding to a green node in Figure 3. Clustering results are shown for the following subsampling/sample sizes: (a) 75/125, 70/117, 60/100 and 55/92; (b) 65/108; (c) 50/83. For better appreciation of the differences of extracted subnetworks relative to that from 80/133 (i.e. the results considered as the 'ground truth'), such differences are indicated with circles of 3 different colors: blue, red and black circles representing the missing brain regions, extra brain regions, and over-clustered clusters (i.e. a cluster is

inappropriately divided into a few clusters at higher levels), respectively. See Table 1 for the definition of node acronyms.

Figure 6: Evaluation of the probability of each extracted subnetwork. The probability values of 13 subnetworks are shown for all 6 subsampling/sample sizes: (a) 50/83; (b) 55/92; (c) 60/100; (d) 65/108; (e) 70/117 & (f) 75/125. On top of each bar, a pair of numbers are shown, representing extracted number of regions/ true number of regions; numbers of such clusters that are inconsistent with ground truth are shown in red color. In addition, a red line corresponding to threshold=0.5 is drawn to show extracted clusters with relatively low threshold (i.e. <0.5).

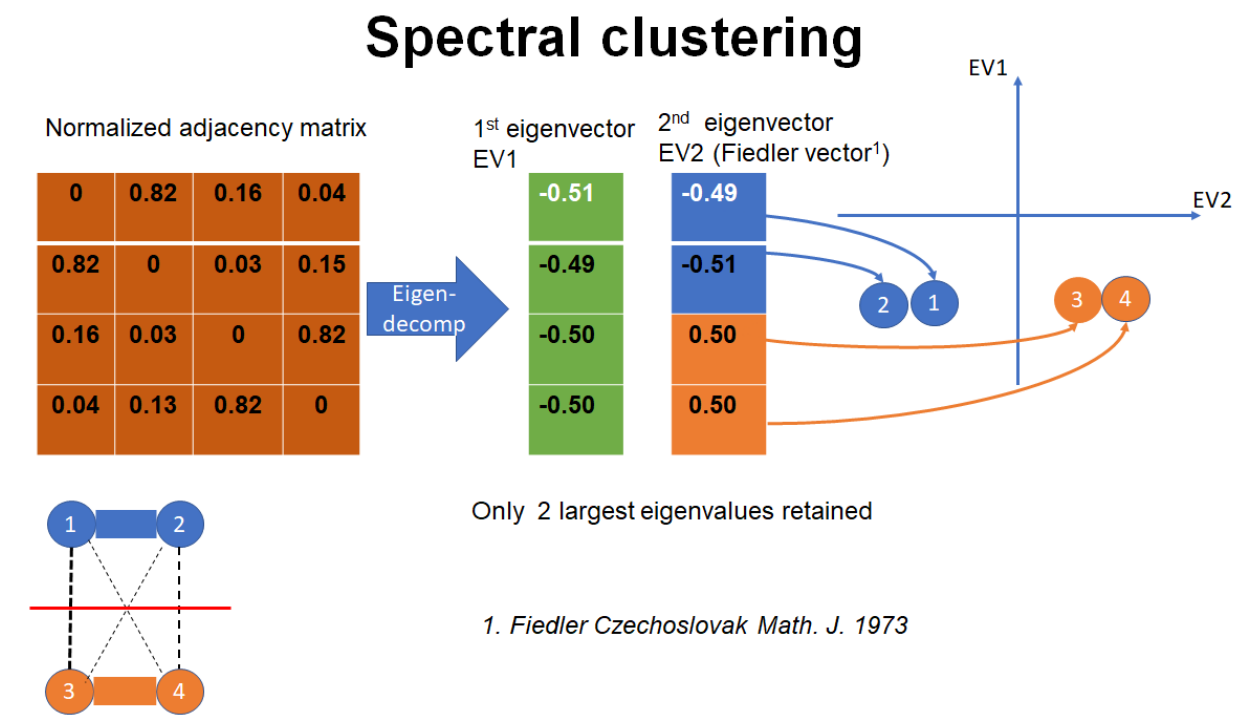
Spectral clustering
Normalized adjacency matrix
0 0.82 0.16 0.04
0.82 0 0.03 0.15
0.16 0.03 0 0.82
0.04 0.13 0.82 0
Eigen-decomp
1st eigenvector EV1
-0.51
-0.49
-0.50
-0.50
2nd eigenvector EV2 (Fiedler vector1)
-0.49
-0.51
0.50
0.50
EV1
EV2
1
2
3
4
Only 2 largest eigenvalues retained
1. Fiedler Czechoslovak Math. J. 1973

Figure 1

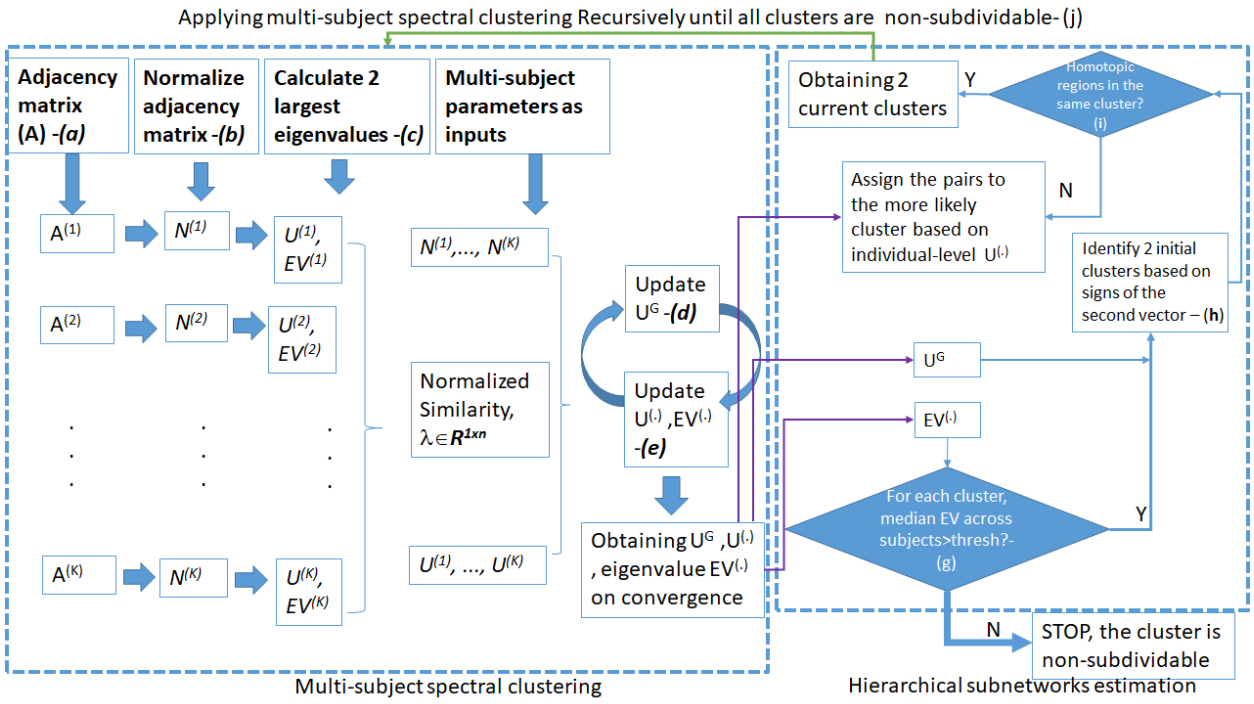
Applying multi-subject spectral clustering Recursively until all clusters are non-subdividable- (j)
Adjacency matrix (A) -(a)
Normalize adjacency matrix -(b)
Calculate 2 largest eigenvalues -(c)
Multi-subject parameters as inputs
A(1)
N(1)
U(1), EV(1)
A(2)
N(2)
U(2), EV(2)
A(K)
N(K)
U(K), EV(K)
N(1),..., N(K)
Normalized Similarity, λ∈R1xn
U(1), ..., U(K)
Update UG -(d)
Update U(.) ,EV(.) -(e)
Obtaining UG ,U(.) , eigenvalue EV(.) on convergence
Multi-subject spectral clustering
Obtaining 2 current clusters
Y
Homotopic regions in the same cluster? (i)
N
Assign the pairs to the more likely cluster based on individual-level U(.)
Identify 2 initial clusters based on signs of the second vector – (h)
UG
EV(.)
For each cluster, median EV across subjects>thresh?- (g)
Y
N
STOP, the cluster is non-subdividable
Hierarchical subnetworks estimation

Figure 2

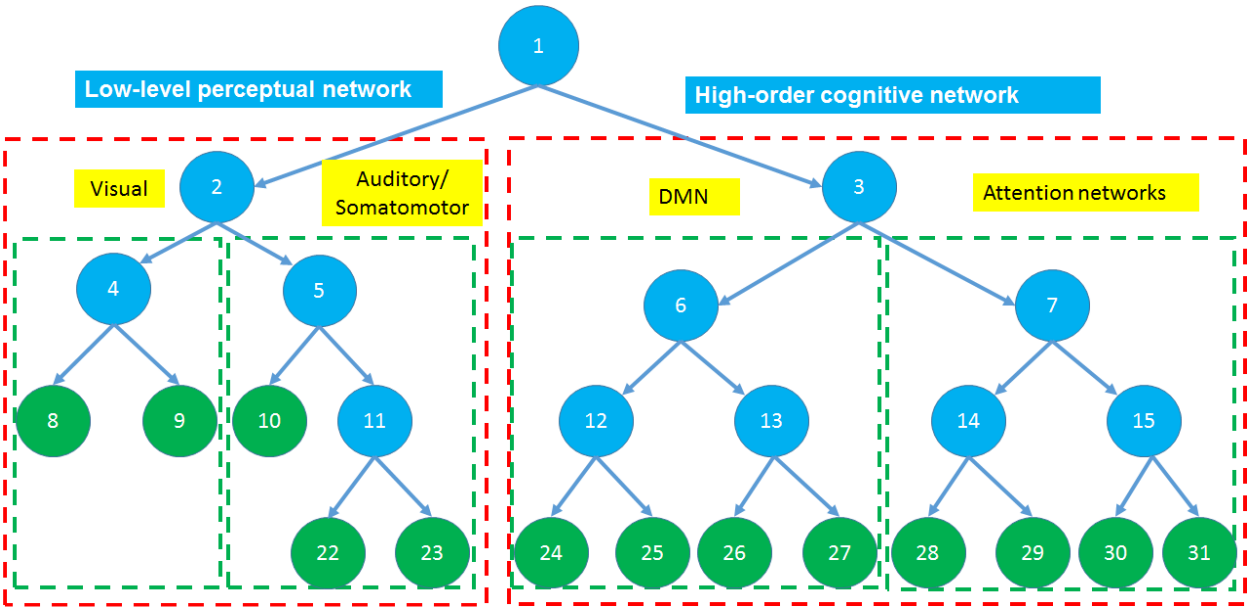
1
Low-level perceptual network
High-order cognitive network
Visual
2
Auditory/
Somatomotor
DMN
3
Attention networks
4
5
6
7
8
9
10
11
12
13
14
15
22
23
24
25
26
27
28
29
30
31

Figure 3

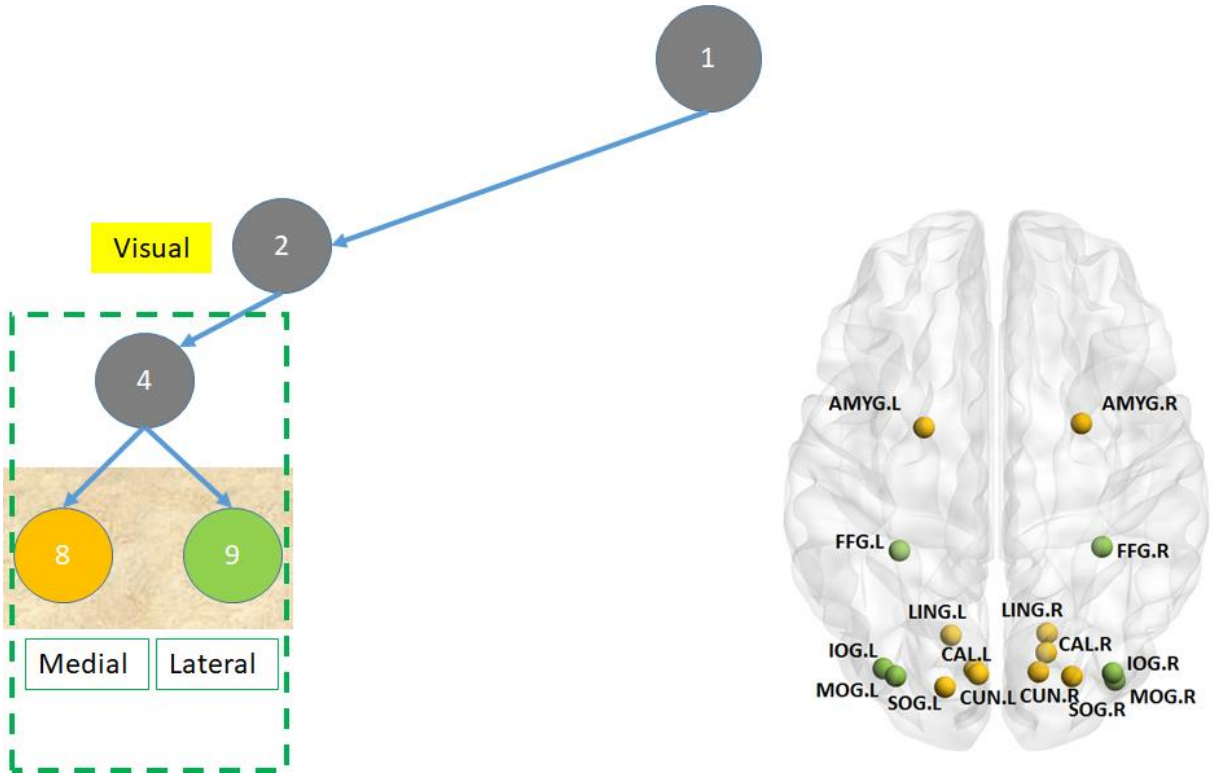

Figure 4(a): Visual networks

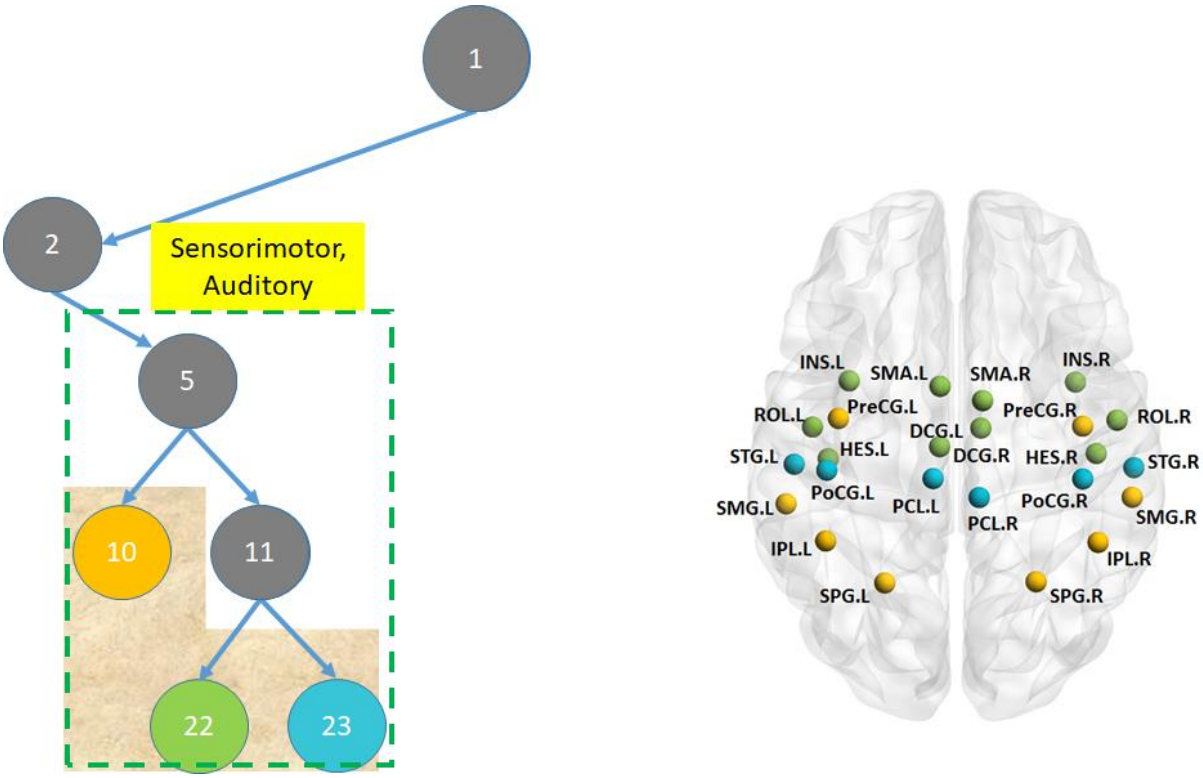

Figure 4(b): Auditory/Somatomotor networks

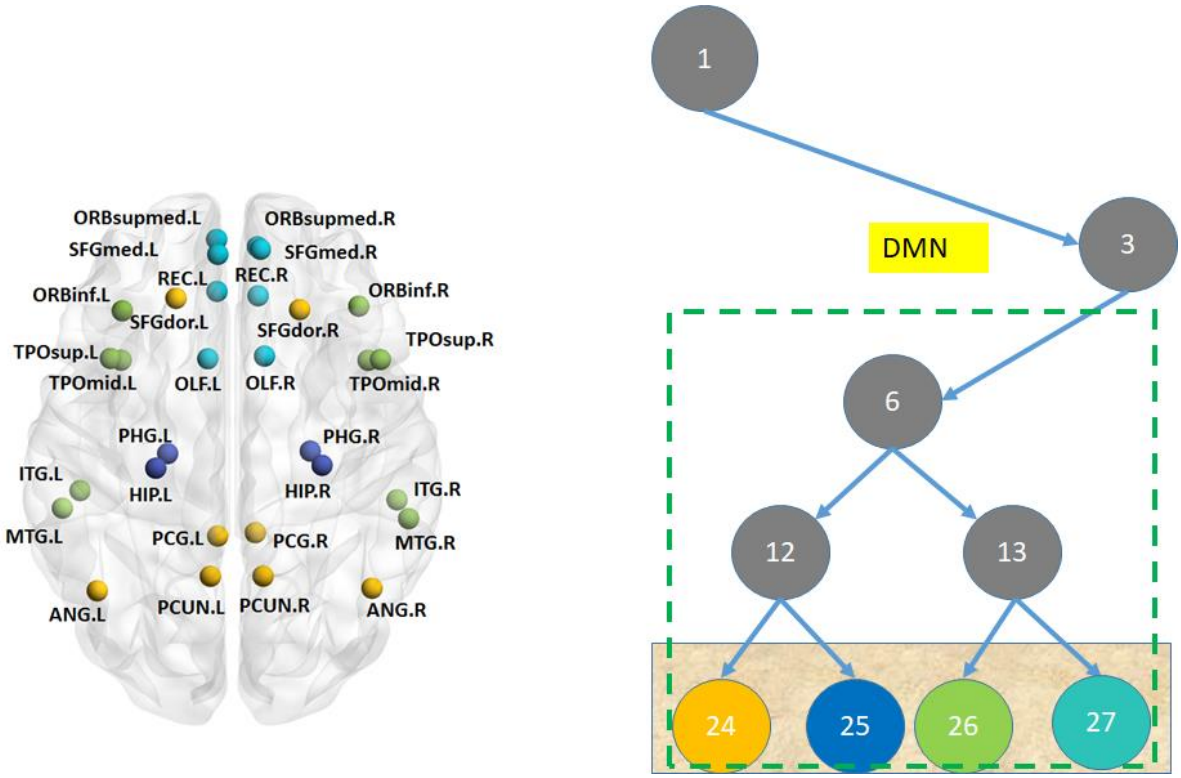

Figure 4(c): Default mode networks

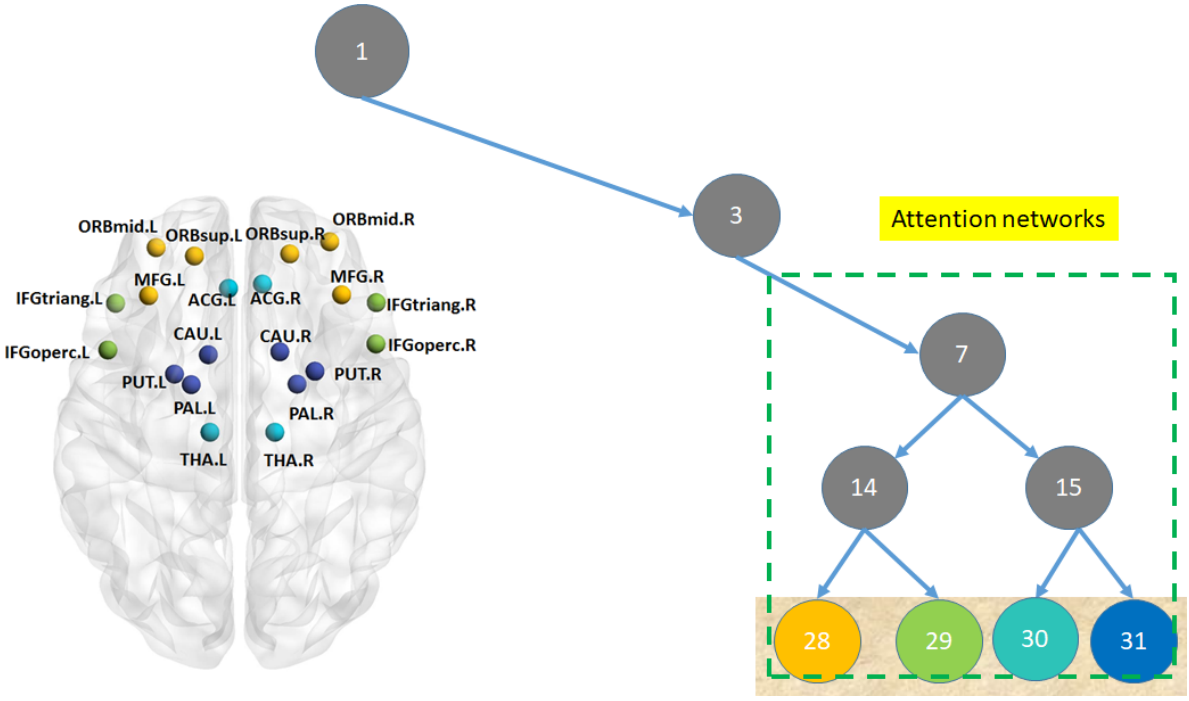

Figure 4(d): Attention networks

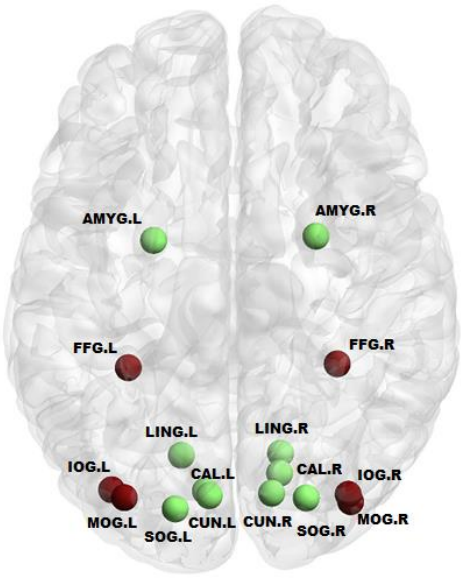

Visual networks

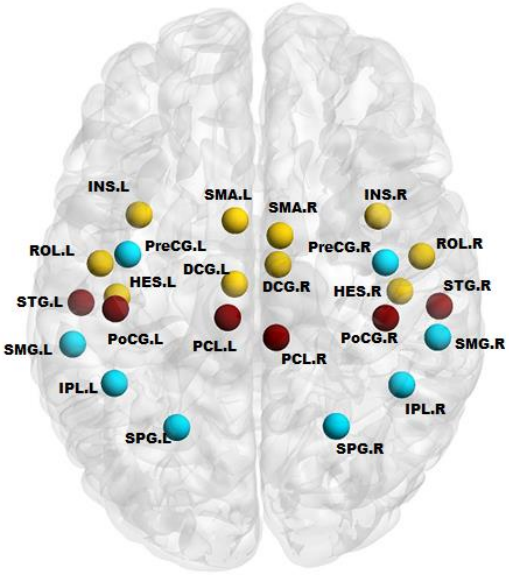

Auditory/somatomotor networks

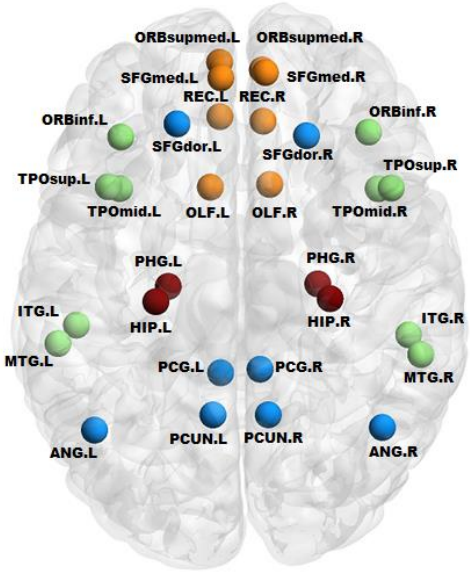

DMN

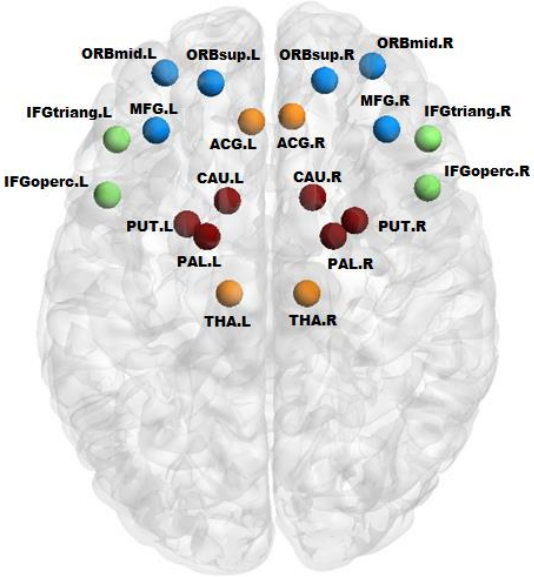

Attention networks

Figure 5(a):

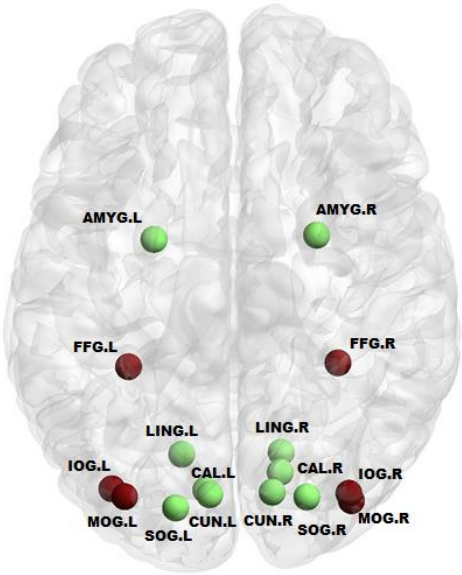

Visual networks

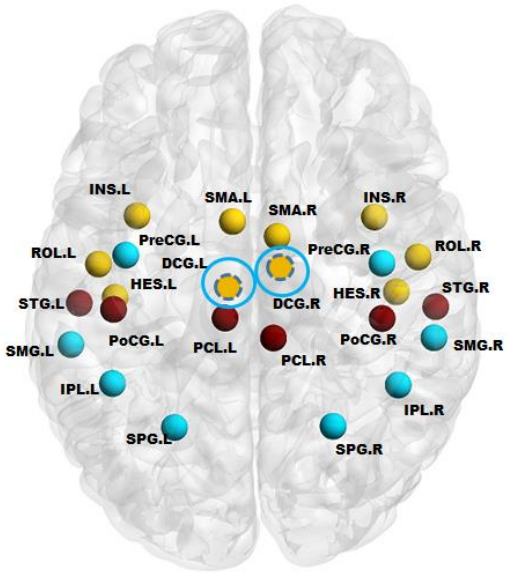

Auditory/Somatomotor networks

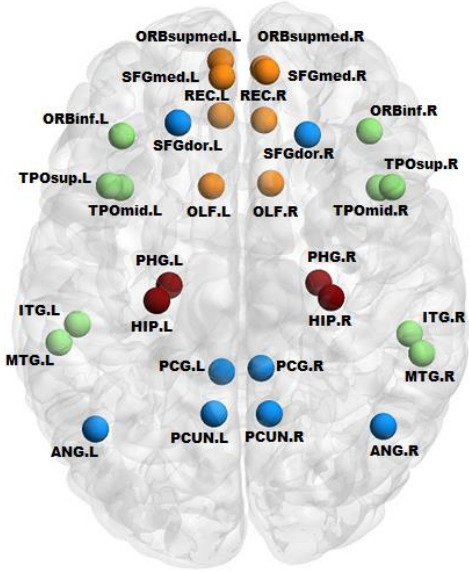

DMN

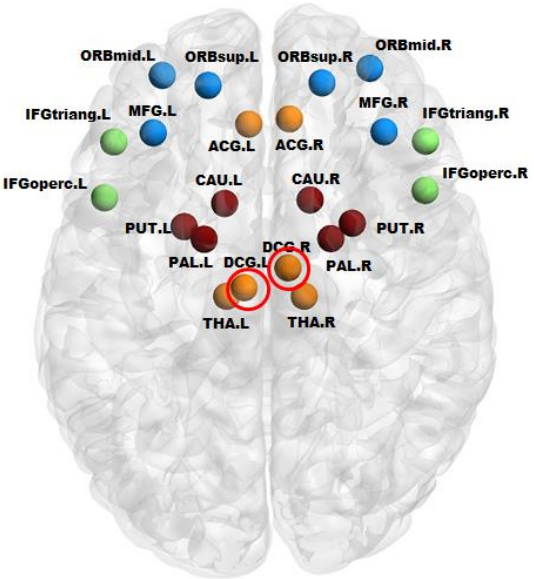

Attention networks

Figure 5(b):

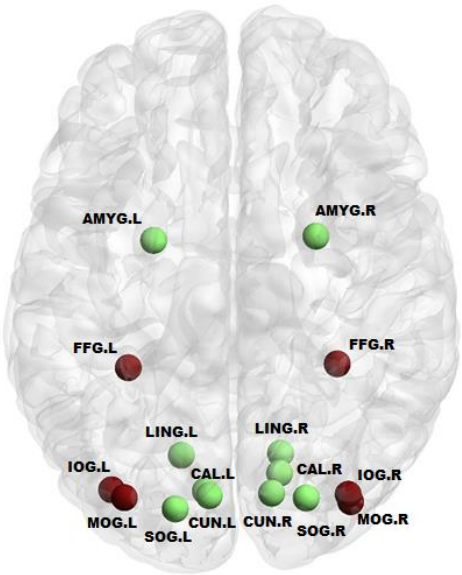

Visual networks

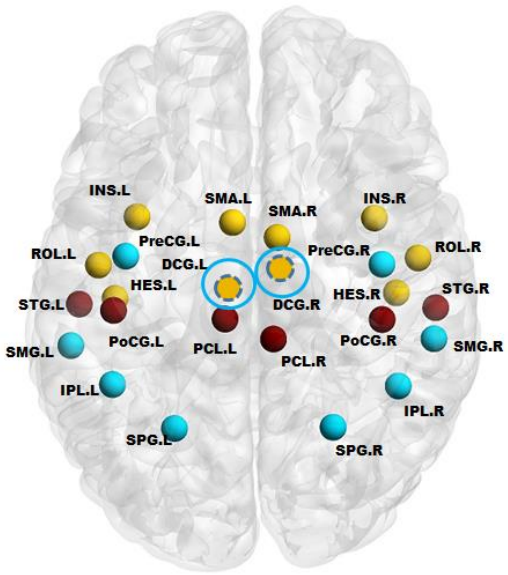

Auditory/somatomotor networks

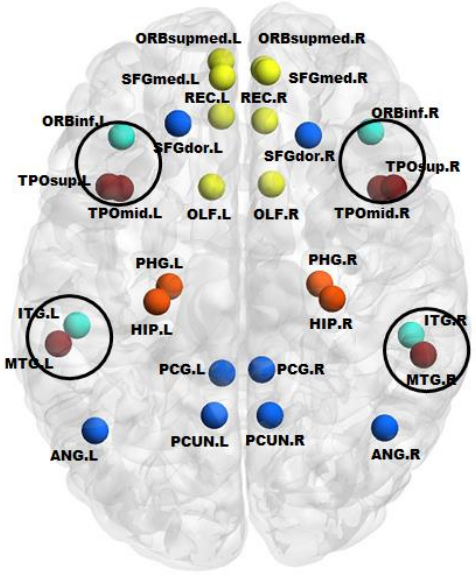

DMN

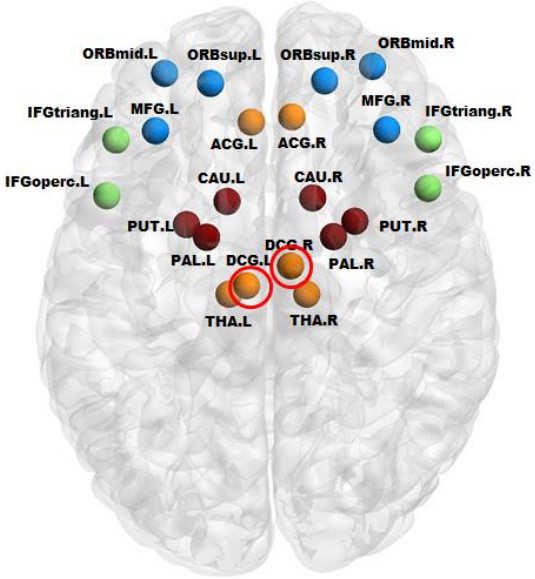

Attention networks

Figure 5(c):

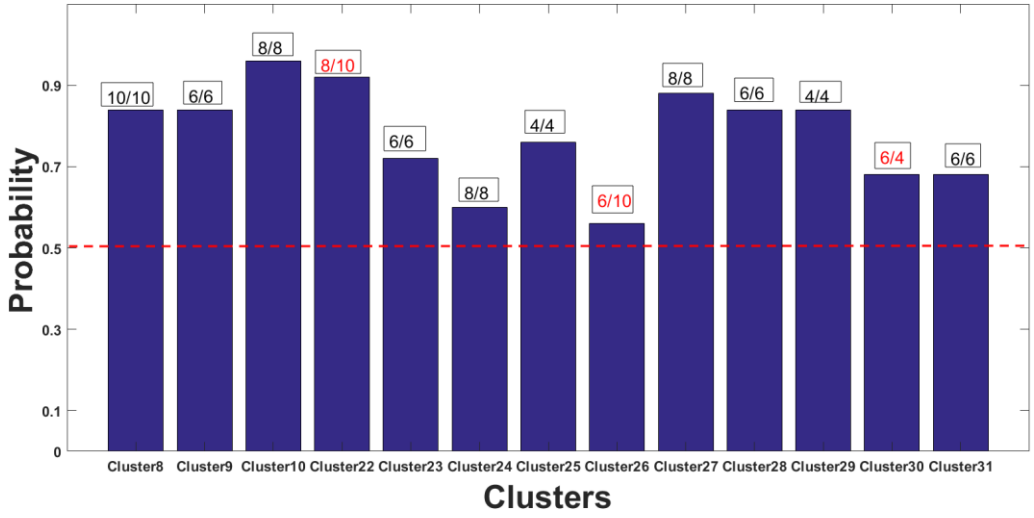

(a) 50/ 83

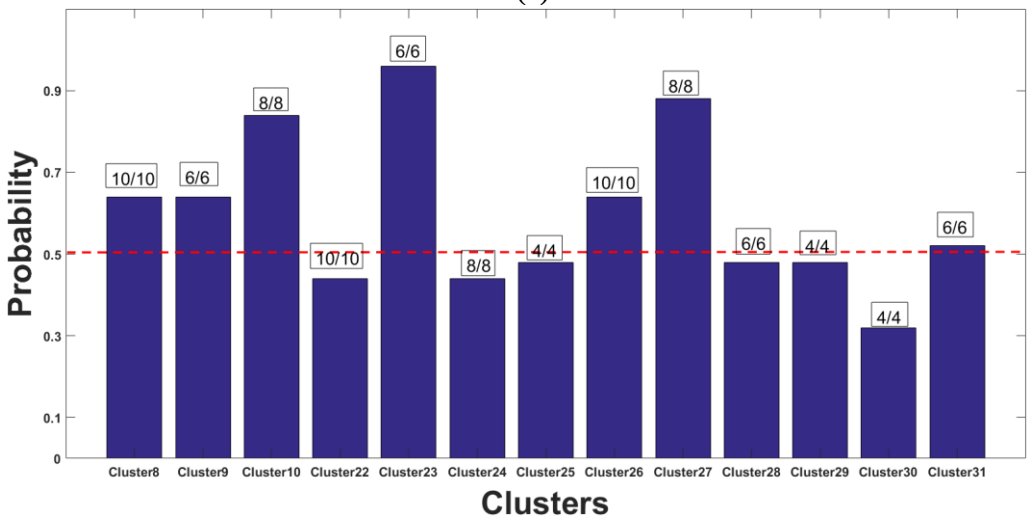

(b) 55/92

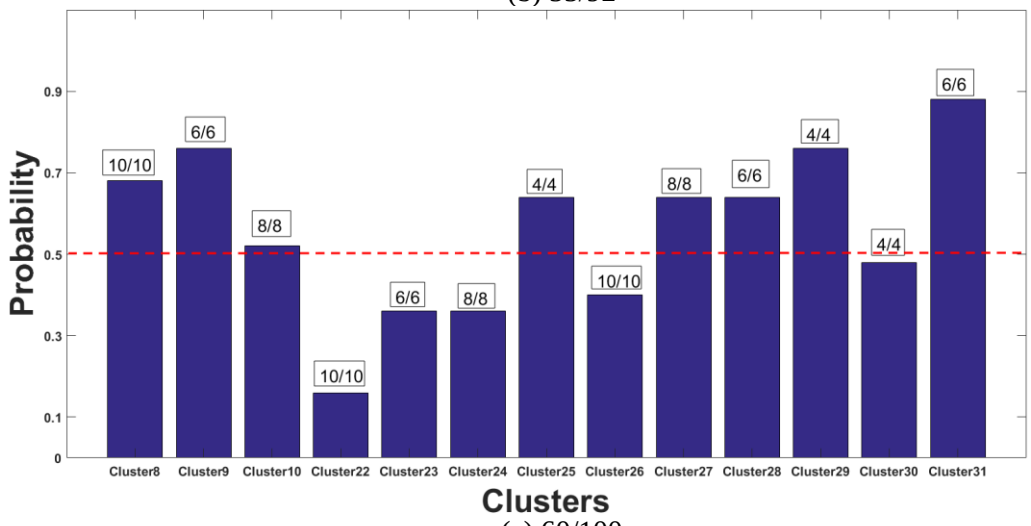

(c) 60/100

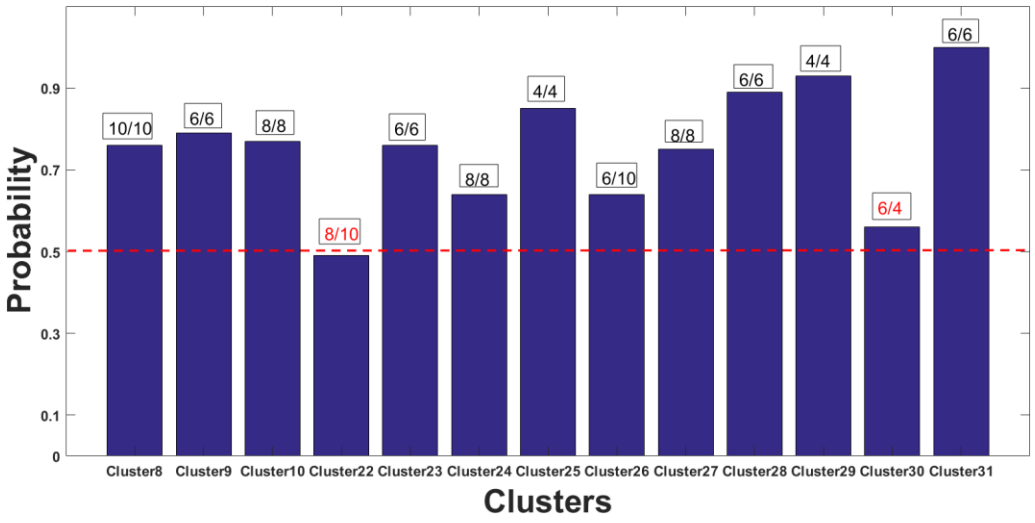

(d) 65/108

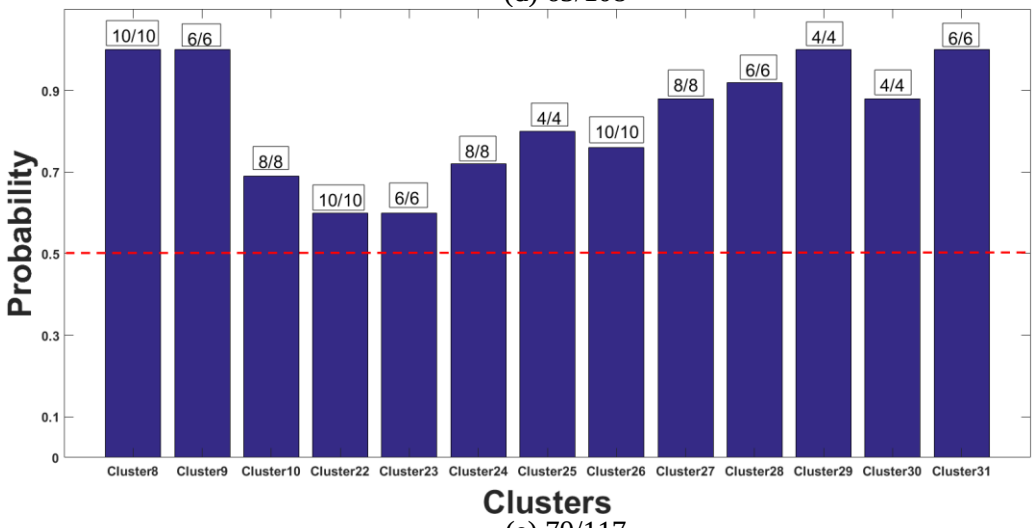

(e) 70/117

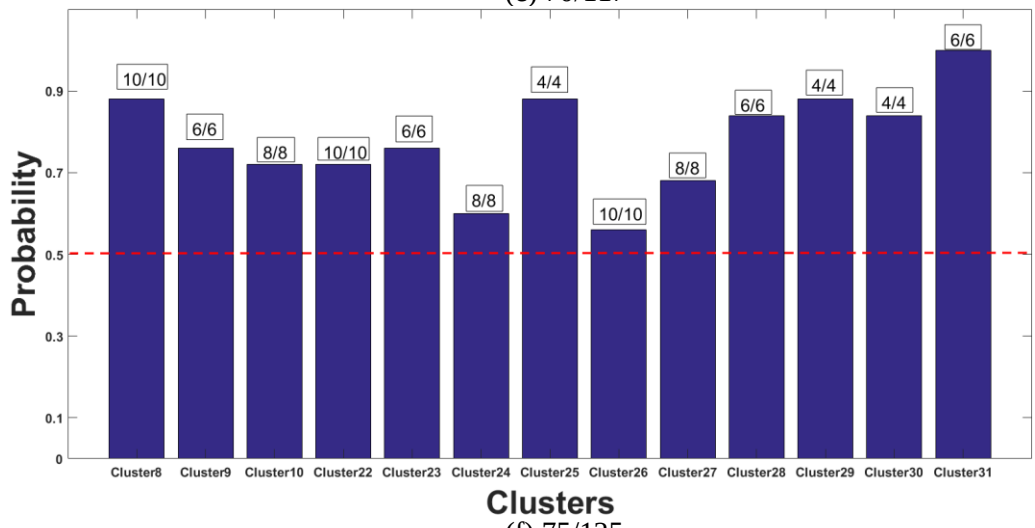

(f) 75/125

Figure 6

Table 1: Brain regions of subnetworks that are consistently extracted from test and retest data for both cases: 75/125 and 80/133 using **NetHiClus** (see Figure 2 and Figure 3). Cluster No. corresponds to the number of indivisible clusters labeled with green color (i.e. the final clustering outcomes) shown in Figure 2. Note: all brain regions are bilaterally present in the related clusters.

Cluster No.	Brain regions in each subnetwork
Cluster 8	Amygdala (AMYG), Calcarine (CAL), Cuneus (CUN), Lingual gyrus (LG), Superior occipital gyrus (SOG)
Cluster 9	Middle occipital gyrus, Inferior occipital gyrus, Fusiform gyrus
Cluster 10	Precentral gyrus (PreCG), Superior parietal gyrus (SPG), Inferior parietal gyrus (IPG), Supramarginal gyrus (SMG)
Cluster 22	Rolandic operculum (ROL), Supplementary motor area (SMA), Insula (INS), Middle cingulum (DCG), Heschl gyrus (HES)
Cluster 23	Postcentral gyrus (PoCG), Paracentral lobule (PCL), Superior temporal gyrus (STG)
Cluster 24	Superior frontal gyrus (SFG), Posterior cingulum (PCG), Angular gyrus (ANG), Precuneus (PCUN)
Cluster 25	Hippocampus (HIP), Parahippocampal gyrus (PHG)
Cluster 26	Inferior frontal-orbital part (ORBinf), Temporal pole-superior part (TPOsup), Middle temporal gyrus (MTG), Temporal pole-middle part (TPOmid), Inferior temporal gyrus (ITG)
Cluster 27	Olfactory (OLF), Superior frontal-medial part (SFGmed), Medial frontal-orbital part (ORBsupmed), Rectus (REC)
Cluster 28	Superior frontal-orbital part (ORBsup), Middle frontal gyrus (MFG), Middle frontal gyrus-orbital part (ORBmid)
Cluster 29	Inferior frontal gyrus-opercular part (IFGoperc), inferior frontal gyrus-triangular part (IFGtriang)
Cluster 30	Anterior cingulum (ACG), Thalamus (THA)
Cluster 31	Caudate (CAU), Putamen (PUT), Pallidum (PAL)